ELSEVIER

European Journal of Pharmaceutics and Biopharmaceutics 55 (2003) 107–113

European Journal of Pharmaceutics and Biopharmaceutics

www.elsevier.com/locate/ejphabio

Research paper

AFM imaging of calixarene based solid lipid nanoparticles in gel matrices

Patrick Shahgaldian[a], Laurence Quattrocchi[a], Jérôme Gualbert[a], Anthony W. Coleman[a,*], Philippe Goreloff[b]

[a]*Institut de Biologie et Chimie des Protéines, Lyon, France*
[b]*Central P bv, Bussum, Netherlands*

Received 15 May 2002; accepted in revised form 6 September 2002

Abstract

Contact mode atomic force microscopy has been carried out on gels of four current polymers, carbopol 980, carbopol 2020, hyaluronic acid and xanthan containing dispersions of solid lipid nanoparticles (SLNs) of amphiphilic calixarenes. Imaging shows that the SLNs are dispersed within the gels as discrete particles of 150 nm in diameter and show little or no aggregation. The simultaneous use of lateral force, topographic and force modulation mode imaging allows a clear interpretation of the observed images, showing the presence of nanoparticles in the sub-surface region and that the SLNs affect the local mechanical properties of the gels. Photon correlation spectroscopy similarly demonstrates a lack of interaction in suspensions.

Keywords: Calixarene; Solid lipid nanoparticles; Atomic force microscopy; Photon correlation spectroscopy; Gel; Carbopol; Hyaluronic acid; Xanthan

1. Introduction

The formulation of drugs is an important topic in pharmaceutical sciences. It aims to improve the bioavailability and the efficiency of active molecules against their target. Many therapeutically active molecules are chemically and biologically fragile, so they need to be encapsulated in a drug carrying system. These systems protect the loaded drug against degradation and the active molecule can be transported effectively in biological media. The development of such systems including micelles [1], liposomes [2], micro- [3] and nanoparticles [4] and solid lipid nanoparticles (SLNs) [5–7] is growing at a fast pace. The SLNs represent one of the most promising class of these colloidal carriers for bioactive molecules. Their advantages over other carrier systems include high temporal and thermal stability [8], high loading capacity [9], ease of preparation [10], low production costs and large scale industrial production. For circulatory applications, their stability as suspensions in the presence of various metabolites and biomacromolecules is a key factor. For topical applications, they must remain as stable, non-aggregated species in gels and emulsifying agents used in the preparation of creams. Such assemblies can be obtained from natural or synthetic molecules. In the field of supramolecular chemistry, amphiphilic crown-ethers [11,12] and cyclodextrins [13–15] have been developed to self-assemble in water as stable particles. Surprisingly, calixarenes which are one of the major synthetic skeletons studied in this field of chemistry have been less studied for their properties to form such assemblies.

Calixarenes [16] (Scheme 1a) are macrocyclic compounds, produced by the base catalyzed reaction of *p*-formaldehyde and *p-tert*-butyl-phenol and their use as bioactive molecules has recently come to the fore. Their activity as ion channel blockers [17], anti-fibrotic [18] and anti-tubercular agents [19] have been shown. More recently, the ability of hydrosoluble calixarenes to complex with albumin [20] has been established. In spite of the large number of amphiphilic calixarenes and resorcinarenes synthesized, only a few reports show their capacity to self-assemble as mesoscopic entities in water. However, Tanaka [21] reported the formation of liposomes by amphiphilic resorcinarenes and Markowitz [22] reported the same for calix[6]arene derivatives.

In a biomimetic approach, we developed the synthesis of amphiphilic calixarenes, analogues of natural phospholipids [23], and studied their ability to form stable nanoparticles in water [24]. Their low production cost and ease of preparation make them good candidates for new systems for drug delivery, especially in cosmetic applications.

* Corresponding author. Institut de Biologie et Chimie des Protéines, CNRS-UMR 5086, 7 passage du Vercors, Lyon F69367, France. Tel.: +33-4-7272-2640; fax: +33-4-7272-2690.
E-mail address: aw.coleman@ibcp.fr (A.W. Coleman).

0939-6411/02/$ - see front matter © 2002 Elsevier Science B.V. All rights reserved.
doi:10.1016/S0939-6411(02)00123-6

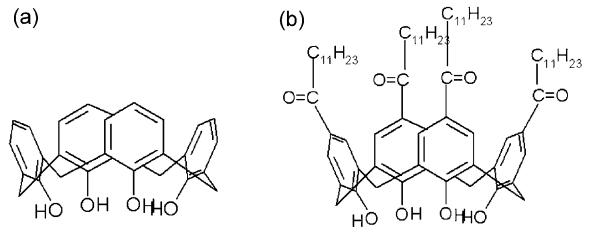

Scheme 1. Formulae of the calix[4]arene (a) and *p*-dodecanoyl-calix[4]arene (b).

In this paper, we report an atomic force microscopy (AFM) study of these nanoparticles incorporated in gels used in cosmetic and dermatological preparations (xanthan, hyaluronic acid, carbopol 980 and carbopol 2020). It will be shown that lateral force and force modulation modes are powerful tools to study the behavior of these particles in gels.

AFM is a key tool in the imaging of soft materials [24], biological systems [25,26] and colloidal systems [27]. It has been applied to the study of liposomes [28], polymeric nano- and microparticles [29] and SLNs [30]. The imaging of natural polymers used in the preparation of topical creams, including hyaluronic acid [31] and xanthan at the molecular level [32] has been reported. The two imaging modes are contact and non-contact modes [33], each containing different sub-modes for which image contrast is generated by different point–surface interactions. These include in the contact mode, topographic (contrast arising from the *Z* motion of the point), error (contrast arising from the feedback signal), lateral force (contrast arising from the signal due to point motion in the *x*–*y* plane and arising from friction forces) and force modulation (contrast arising from damping of a low frequency (5 kHz) oscillation applied to the cantilever and reacting to local variations in the mechanical strength of the signal). The use of simultaneous imaging in the several sub-modes allows analysis of various properties of the surface, and in the case of force modulation the sub-surface of a sample, and allows a detailed analysis of the nature and local properties of a sample to be obtained rapidly.

In this paper, we report multi-mode contact AFM imaging of calixarene based nanoparticles dispersed in various gels used in topical preparations, including hyaluronic acid, xanthan, carbopol 980 and carbopol 2020. It will be shown that the calixarene based SLNs are present as non-aggregated particles in the gels. The use of lateral force and force modulation modes in addition to the classical topographic mode will be shown to provide additional information on the gel structuring and the presence of nanoparticles in the gels.

2. Experimental

2.1. SLN preparation

p-Dodecanoyl-calix[4]arene (Scheme 1(b)) was synthesized as previously described [23]. The SLNs were prepared by the solvent displacement method [14]. *p*-Dodecanoyl-calix[4]arene was dissolved in tetrahydrofuran (THF) at a concentration of 5 mg/ml. To 3 ml of this solution, under magnetic stirring at a constant rotation speed of 300 rpm, 100 ml of pure water (resistivity >18 MΩ cm) was added at a flow rate of 300 ml/min. The slightly milky suspension was stirred for another 1 min. THF was evaporated under reduced pressure at 40°C, using a rotary evaporator and the suspension was concentrated to a final volume of 10 ml, yielding a final SLN concentration of 1.5 g/l.

2.2. Sample preparation

Carbopol 980, carbopol 2020, xanthan and hyaluronic acid were hydrated in water at a concentration of 0.5% for 1 h at room temperature under magnetic stirring. A volume of 0.5 ml of the nanoparticle suspensions was mixed with an equal volume of the gels giving a final concentration of calixarene of 750 mg/l. The samples were prepared by depositing a volume of 20 μl of these mixtures on freshly cleaned microscopic slides and were dried overnight at room temperature. The blanks were prepared in a similar way by diluting the gel with pure water.

2.3. Photon correlation spectroscopy (PCS)

The size of the nanoparticles was measured by PCS using a Malvern spectrometer (Malvern, UK) and 71320256 channel correlator with a 40 mW He–Ne (633 nm) laser. The measurements were carried out on diluted gels.

2.4. AFM experiments

Imaging was carried out using a Thermomicroscope Explorer AFM (Thermomicroscopes Inc., Santa Clara, USA) equipped with a 100 μm tripod scanner, in contact mode, using pyramidal cantilevers with silicon probes (force constant: 0.032–0.064 N/m) at a scan frequency of 1 Hz, and applied forces were of the order of 0.3–1.2 nN.

For all samples, lateral force and force modulation acquisition were run independently, in both cases, topographic

Table 1
Average hydrodynamic diameter (nm) measured by PCS on the diluted SLNs suspensions in water or gels

	Water	Carbopol 980	Carbopol 2020	Hyaluronic acid	Xanthane
Average diameter (nm)	137	140	146	165	155

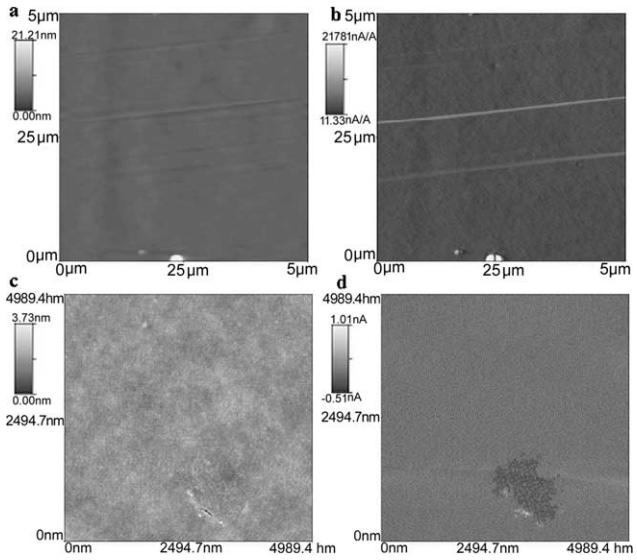

Fig. 1. AFM images, at 5 μm scan range, of hyaluronic acid in (a and c) topographic mode, (b) force modulation mode and (d) lateral force mode. Images a + b and c + d were collected simultaneously.

and internal sensor forward images were collected simultaneously, sequentially from 50×50, 25×25, 10×10 μm to 5×5 μm. Images are processed with the SPMLab 5.01 software package and are presented unfiltered.

2.5. Roughness analysis

The calculated roughness values are derived from the Thermomicroscope SPML 5.01 software package. The average roughness (R_a) is defined as the arithmetic mean of the deviations in height Eq. (1) and the root mean square roughness (RMS) defined as the square root of the mean value of the squares of the distance of the points from the image mean value Eq. (2) and the average height of the sample Eq. (3)

$$R_a = \frac{1}{N}\sum_{i=1}^{N}|z_i - \bar{z}| \quad (1)$$

$$\mathrm{RMS} = \sqrt{\frac{1}{N}\sum_{i=1}^{N}\langle z_i - z\rangle^2} \quad (2)$$

$$\text{Avg. height} = \frac{1}{N}\sum_{i=1}^{N} z_i \quad (3)$$

3. Results and discussion

In order to probe possible interactions between the SLNs and the various gels in the suspensions, prior to deposition, PCS measurements were carried out on the calixarene based SLNs alone, the diluted polymer gels and diluted mixtures of SLNs and polymer gels. Particle size peaks occurring in the diluted polymer gel samples were ignored in treating the PCS results for the mixed systems. The results of the particle sizes for the SLNs are reported in Table 1. The size varies from 137 nm for the SLNs alone to 140, 146, 165 and 155 nm for the mixed system with carbopol 980, carbopol 2020, hyaluronic acid and xanthan, respectively. Within the limits of the experiment no effective size is increased, and we postulate that no specific polymer–SLN interactions were observed in the systems studied here.

Figs. 1–4 show the images of the gels without nanoparticles in topographic (a, c), force modulation (b) and lateral force (d) modes, for hyaluronic acid, xanthan, carbopol 980 and carbopol 2020, respectively, at a scan range of 5 μm; images a + b and c + d were collected simultaneously. The

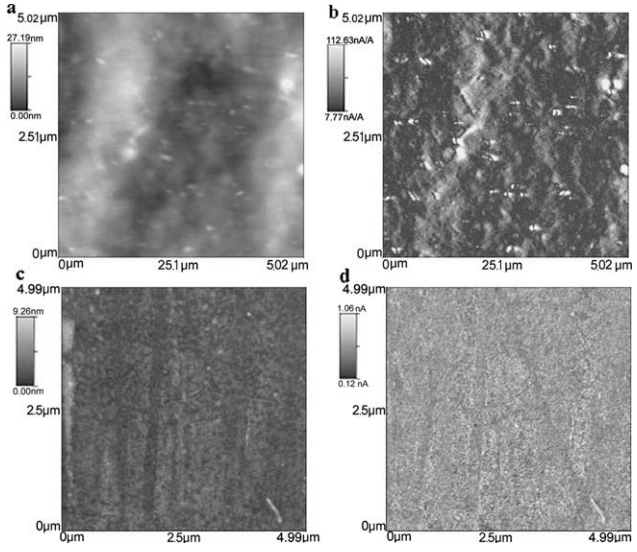

Fig. 2. AFM images, at 5 μm scan range, of xanthan in (a and c) topographic mode, (b) force modulation mode and (d) lateral force mode. Images a + b and c + d were collected simultaneously.

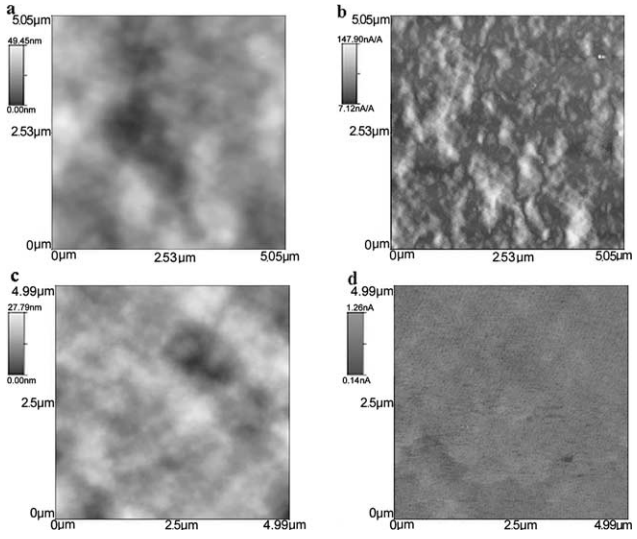

Fig. 3. AFM images, at 5 μm scan range, of carbopol 980 in (a and c) topographic mode, (b) force modulation mode and (d) lateral force mode. Images a + b and c + d were collected simultaneously.

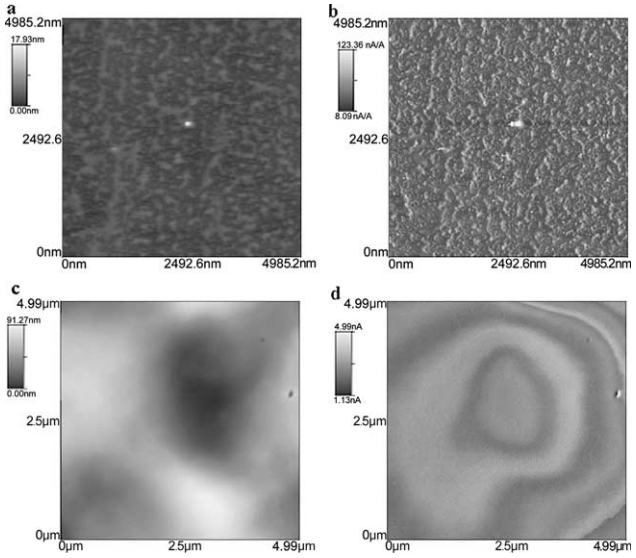

Fig. 4. AFM images, at 5 μm scan range, of carbopol 2020 in (a and c) topographic mode, (b) force modulation mode and (d) lateral force mode. Images a + b and c + d were collected simultaneously.

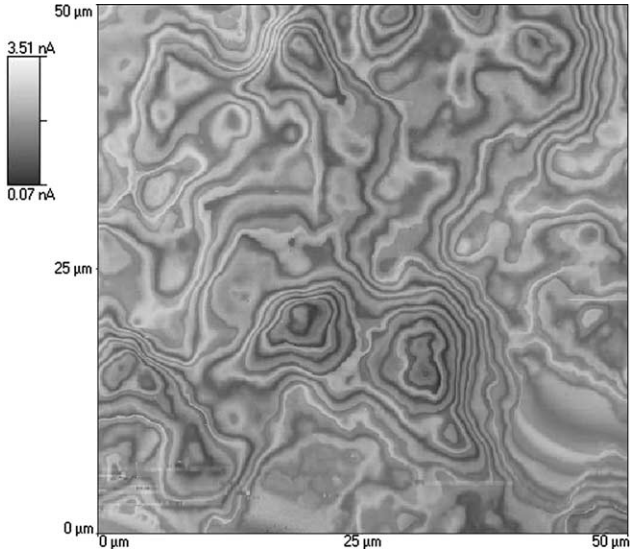

Fig. 5. Lateral force image, at 50 μm scan range of the gel of carbopol 2020.

area roughness analyses of these films, obtained from the topographic images are given in Table 2.

Of the four gels, carbopol 2020 shows significantly the roughest surface with a RMS roughness of 71 nm over a $10 \times 10\ \mu m^2$ area. The other three gels are effectively planar with RMS values of 9.6, 3.8, and 10.1 nm for hyaluronic acid, xanthan and carbopol 980, respectively.

Each system shows different topography; carbopol 980 shows a surface of elevated and valley features, while carbopol 2020 shows a rippled surface oriented effectively in the *y* axis of the image.

The surface of hyaluronic acid is essentially flat, while a 'hill and valley' topography is observed for the xanthan gel. The error images in each case (data not shown), provide essentially the same information except that the visual contrast is improved.

The lateral force images (Figs. 1d–4d) show essentially no contrast for the samples carbopol 980, xanthan and hyaluronic acid. The slight contrast for carbopol 980 arises undoubtedly from some cross-talk between the topographic image and the lateral force image. This lack of contrast is a clear evidence for the essentially homogeneous nature of the samples. In the case of carbopol 2020, there are apparent moiré rings in the 5 μm image. The lateral force microscopy image (LFM) at a 50 μm scan range is given in Fig. 5. Here, a large number of moiré patterns are visible, these have been previously observed by us in a partially annealed film of *iso*-propyl calix[6]arene, and are believed to arise from locally differing surface forces due to stress induced in films during deposition [34].

The force modulation microscopy (FMM) images (Figs. 1b–4b) in all cases show no features that are not present in the topographic images.

In Figs. 6–9 are given the images of the four gels,

Table 2
Roughness analysis of the four gels, hyaluronic acid, xanthan, carbopol 980 and carbopol 2020, calculated at scan ranges of 10 μm, where R_a is the mean roughness and RMS is the RMS roughness; values are expressed in nanometer

Compound	Area R_a	RMS	Avg height	Maximum range
Hyaluronic acid	8.0	9.6	32.8	48.8
Xanthan	3.0	3.8	15.6	46.2
Carbopol 980	7.9	10.1	35.8	71.1
Carbopol 2020	55.1	70.7	179.0	395.6

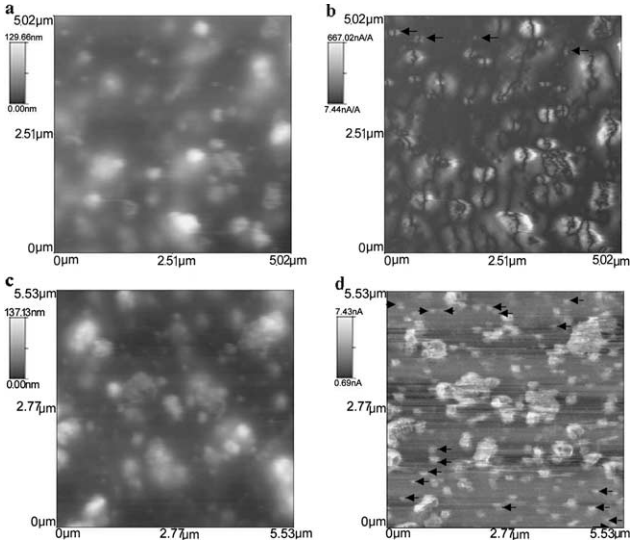

Fig. 6. AFM images, at 5 μm scan range, of hyaluronic acid containing nanoparticles in (a and c) topographic mode, (b) force modulation mode and (d) lateral force mode. Images a + b and c + d were collected simultaneously. The SLNs not observed in topographic modes, but observed in LFM and FMM are marked with horizontal arrows.

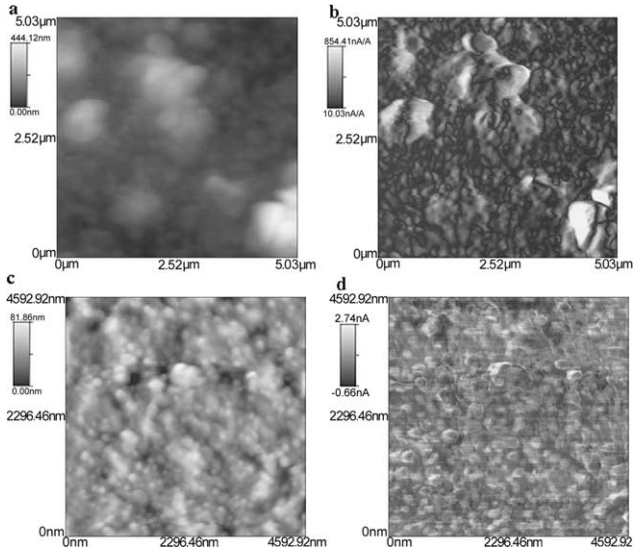

Fig. 7. AFM images, at 5 µm scan range, of xanthan containing nanoparticles in (a and c) topographic mode, (b) force modulation mode and (d) lateral force mode. Images a + b and c + d were collected simultaneously.

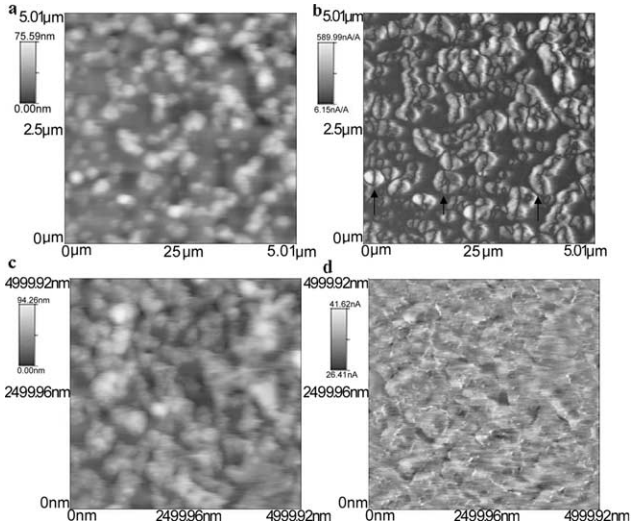

Fig. 9. AFM images, at 5 µm scan range, of carbopol 2020 containing nanoparticles in (a and c) topographic mode, (b) force modulation mode and (d) lateral force mode. Images a + b and c + d were collected simultaneously. The 'coffee grain' structures are marked with vertical arrows.

hyaluronic acid, xanthan, carbopol 980 and carbopol 2020, respectively, containing dispersions of the calixarene based SLNs. In all the cases, the sample treatment and gel concentration are identical to those above. The area roughness analysis is given in Table 3; the RMS roughness increases from 8 to 15 nm, 8 to 58 nm, and 3 to 17 nm for hyaluronic acid, carbopol 980 and xanthan, respectively, in the absence and presence of the SLNs. In contrast, the RMS value for carbopol 2020 decreases from 55 to 33 nm. Thus, in all cases the presence of the SLNs within the gels is easily detected in the contact mode AFM images. The increase in the RMS values for hyaluronic acid, carbopol 980 and xanthan is due to the presence of the SLNs at the surface, and the increase also occurs for carbopol 2020. However, in this case, the RMS for the pure gel is much greater and effective even though the SLNs protrude out from the surface, a lower overall sample roughness results in the lower observed RMS.

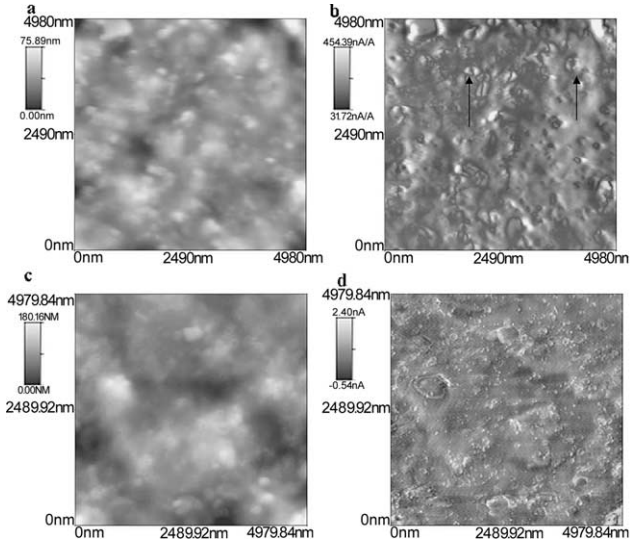

Fig. 8. AFM images, at 5 µm scan range, of carbopol 980 containing nanoparticles in (a and c) topographic mode, (b) force modulation mode and (d) lateral force mode. Images a + b and c + d were collected simultaneously. The 'coffee grain' structures are marked with vertical arrows.

While the presence of SLNs at the surface can be seen in the topographic images (Figs. 6a, c–9a, c), they are much more clearly apparent in the force modulation (Figs. 6b–9b) and lateral force modes (Figs. 6d–9d). The size of the observed SLNs has been determined using the line analysis sub-routine in the SPML 5.01 and the results are summarized in Table 4.

The LFM images (Figs 6d–9d) show the presence of nanoparticles (horizontal arrows) that are not observed in the topographic mode image. These are clearly SLNs which are just below the surface of the gels. While these SLNs affect only marginally or not all the topography, they change locally, by modifying the surface forces, the point–surface interactions in the lateral force mode, and hence, may be observed.

As with the lateral force images, in the force modulation

Table 3
Roughness analysis of the four gels, hyaluronic acid, xanthan, carbopol 980 and carbopol 2020, calculated on samples containing calixarene nanoparticles at scan ranges of 10 µm, where R_a is the mean roughness and RMS is the RMS roughness, values are expressed in nano meter

Compound	Area R_a	RMS	Avg height	Maximum range
Hyaluronic acid	15.4	21.4	25.6	202.2
Xanthan	17.0	22.8	53.4	213.3
Carbopol 980	58.8	80.1	259.5	676.2
Carbopol 2020	33.5	42.7	108.9	370.0

Table 4
Average diameter and height of the SLNs, observed in hyaluronic acid, xanthan, carbopol 980 and carbopol 2020 gels, calculated using the line analysis subroutine in the SPML 5.01 software; values are expressed in nanometers

Without gel		Hyaluronic acid		Xanthan		Carbopol 980		Carbopol 2020	
Average diameter	Average height	Average diameter	Average height	Average diameter	Average height	Average diameter	Average height	Average diameter	Average height
185	47	170	152	163	186	179	192	202	224

images (Figs. 6b–9b) the presence of SLNs in the gel matrix and those which do not appear in the topographic image may readily be detected and are marked by horizontal arrows. Effectively in all four gels these appear as 'coffee grain structures', for clarity, examples are marked by vertical arrows in Figs. 8 and 9. The interactions between SLNs and the gel matrix, even for systems quite deeply embedded in the gel leads to a modification in the mechanical strength. The diameter of the observed SLNs in the force modulation mode is about 100–160 nm larger than the observed topographic diameter. This is expected due to propagation of the changes in mechanical properties into the gel matrix, which are in the range of 50–80 nm.

Finally it is interesting to note that successful contact mode imaging of the gels and the SLN containing gels in air is achieved with relative facility as these systems are relatively soft materials.

4. Conclusion

In conclusion, the presence of non-aggregated calixarene based SLNs in four gels have been demonstrated by contact mode AFM imaging. The use of multi-mode imaging allows clear visualization of the SLNs at the surface by topographic and error modes. From the lateral force and force modulation images, SLNs which are not involved in surface features can be observed due to their effects on local surface forces and the local mechanical properties of the gels. The lack of polymer–SLN interactions is confirmed by PCS.

Acknowledgements

One of us, P.S., thanks Central P BV for financial support. We acknowledge the financial aid of the FRM for the Atomic Force Microscope and a grant for P.S.

References

[1] K. Kataoka, A. Harada, Y. Nagasaki, Block copolymer micelles for drug delivery: design, characterization and biological significance, Adv. Drug Deliv. Rev. 47 (2001) 113–131.
[2] Y.-P. Zhang, B. Ceh, D.D. Lasic, Liposomes in drug delivery, in: D. Severian (Ed.), Polymeric Biomaterials, 2nd ed., Marcel Dekker, New York, NY, 2002, pp. 783–821.
[3] H. Kawaguchi, Functional polymer microspheres, Prog. Polym. Sci. 25 (2000) 1171–1210.
[4] R. Alvarez-Roman, G. Barre, R.H. Guy, H. Fessi, Biodegradable polymer nanocapsules containing a sunscreen agent: preparation and photoprotection, Eur. J. Pharmacol. Biopharmacol. 52 (2001) 191–195.
[5] W. Mehnert, K. Mader, Solid lipid nanoparticles; production, characterization and applications, Adv. Drug Deliv. Rev. 47 (2001) 165–196.
[6] R.H. Müller, W. Mehnert, J.S. Lucks, C. Schwarz, A. zur Mühlen, H. Weyhers, C. Freitas, D. Rühl, Solid lipid nanoparticles (SLN)—an alternative colloidal carrier system for controlled drug delivery, Eur. J. Pharmacol. Biopharmacol. 41 (1995) 62–69.
[7] R.H. Müller, K. Mäder, S. Gohla, Solid lipid nanoparticles (SLN) for controlled drug delivery – a review of the state of the art, Eur. J. Pharmacol. Biopharmacol. 50 (2000) 161–177.
[8] H. Heiati, R. Tawashi, N.C. Philips, Drug retention and stability of solid lipid nanoparticles containing azidothymidine palmitate after autoclaving, storage and lyophilization, J. Microencapsul. 15 (1998) 173–184.
[9] A. zur Mühlen, C. Schwarz, W. Mehnert, Solid lipid nanoparticles (SLN) for controlled drug delivery – drug release and release mechanism Eur, J. Pharmacol. Biopharmacol. 45 (1998) 149–155.
[10] A. Lippacher, R.H. Müller, K. Mader, Preparation of semisolid drug carriers for topical application based on solid lipid nanoparticles, Int. J. Pharmacol. 214 (2001) 9–12.
[11] S.L. De Wall, L.J. Barbour, G.W. Gokel, Solid-state bilayer formation from a dialkyl-substituted lariat ether that forms stable vesicles in aqueous suspension, J. Phys. Org. Chem. 14 (2001) 383–391.
[12] I.A. Darwish, F.I. Uchegbu, The evaluation of crown ether based niosomes as cation containing and cation sensitive drug delivery systems, Int. J. Pharmacol. 159 (1997) 207–213.
[13] D. Duchêne, G. Ponchel, D. Wouessidjewe, Cyclodextrins in targeting; application to nanoparticles, Adv. Drug. Deliv. Rev. 36 (1999) 29–40.
[14] N. Terry, D. Rival, E. Perrier, A.W. Coleman, Use of cyclodextrin derivatives for skin preparations, etc., their micelles or nanoparticles, and compositions containing the derivatives, French Patent, FR 2000-6102, 2001.
[15] B.J. Ravoo, R. Darcy, Cyclodextrin bilayer vesicles, Angew. Chem., Int. Ed. 39 (2000) 4324–4326.
[16] C.D. Gutsche, in: J.F. Stoddart (Ed.), Calixarenes Revisited, The Royal Society of Cambridge, Cambridge, UK, 1998.
[17] G. Droogmans, J. Prenen, J. Eggermont, T. Voets, B. Nilius, Voltage-dependent block of endothelial volume-regulated anion channels by calix[4]arenes, Am. J. Physiol. 275 (1998) 646–652.
[18] E. Aubert-Foucher, D.J.S. Hulmes, A.W. Coleman, Use of calix(n)arenes for treating fibrotic diseases, French Patent FR 98-10074 19980805, 1998.
[19] P.D. Hart, J.A. Armstrong, E. Brodaty, Calixarenes with host-mediated potency in experimental tuberculosis: further evidence that macrophage lipids are involved in their mechanism of action, Infect. Immun. 64 (1996) 1491–1493.
[20] L. Memmi, A. Lazar, A. Brioude, V. Ball, A.W. Coleman, Protein–calixarene interactions: complexation of bovine serum albumin by sulfonatocalix[n]arenes, J. Chem. Soc. Chem. Commun. (2001) 2474–2475.
[21] Y. Tanaka, M. Miyachi, Y. Kobuke, Selective vesicle formation from

calixarenes by self assembly, Angew. Chem. Int. Ed. 38 (1999) 504–506.
[22] M.A. Markowitz, R. Bielski, S.L. Regen, Ultrathin monolayers and vesicular membranes from calix[6]arenes, Langmuir 5 (1989) 276–278.
[23] P. Shahgaldian, A.W. Coleman, V.I. Kalchenko, Synthesis and properties of novel amphiphilic calix-[4]-arene derivatives, Tetrahedron Lett. 42 (2001) 577–579.
[24] P. Shahgaldian, M. Cesario, P. Goreloff, A.W. Coleman, Para-acyl calix[4]arenes: amphiphilic self-assembly from the molecular to the mesoscopic level, J. Chem. Soc. Chem. Commun. (2002) 326–327.
[25] J.A. DeRose, J.-P. Revel, Studying the surface of soft materials (live cells) at high resolution by scanning probe microscopy: challenges faced, Thin Solid Films 331 (1998) 194–202.
[26] D. Fotiadis, S. Scheuring, S.A. Müller, A. Engel, D.J. Müller, Imaging and manipulation of biological structures with the AFM, Micron 33 (2002) 385–397.
[27] M.R. Yalamanchili, S. Veeramasuneni, M.A.D. Azevedo, J.D. Miller, Use of atomic force microscopy in particle science and technology research, Colloids Surf. A 133 (1998) 77–88.
[28] M.H. Paclet, A.W. Coleman, S. Vergnaud, F. Morel, P67-phox-mediated NADPH oxidase assembly: imaging of cytochrome b558 liposomes by atomic force microscopy, Biochemistry 39 (2000) 9302–9310.
[29] I. Montasser, H. Fessi, A.W. Coleman, AFM imaging of novel type of polymeric colloidal nanostructures, Eur. J. Pharmacol. Biopharmacol. (2002) (in press).
[30] A. zur Müehlen, E. zur Müehlen, H. Niehus, W. Mehnert, Atomic force microscopy studies of solid lipid nanoparticles, Pharmacol. Res. 13 (1996) 1411–1416.
[31] I. Jacoboni, U. Valdre, G. Mori, D. Quaglino Jr, I. Pasquali-Ronchetti, Hyaluronic acid by atomic force microscopy, J. Struct. Biol. 126 (1999) 52–58.
[32] T.A. Camesano, A. Terri, K.J. Wilkinson, Single molecule study of xanthan conformation using atomic force microscopy, Biomacromolecules 2 (2001) 1184–1191.
[33] R. Wiesendanger, Scanning Probe Microscopy, Methods and Applications, Cambridge University Press, Cambridge, UK, 1994.
[34] P. Shahgaldian, P. Goreloff, R. Lamartine, A.W. Coleman, An SPM study of time dependent crystallization processes in iso-propyl-calix-[6]-arene thin films, Cryst. Eng. 5 (2002) 47–58.